may prevent the induction of ER chaperone. No compensatory increase in the ER chaperone may deteriorate the ER function to cope with ER stress when proteasome activity is inhibited (*Figure 6*).

In the present study, proteasome inhibition activated ER-initiated apoptotic signalling such as CHOP, caspase-12, and JNK. Using siRNA targeting CHOP and pharmacological inhibitors for caspase-12 and JNK, we found that CHOP knockdown partially, but significantly, inhibited cardiac apoptosis, while other pharmacological inhibitors did not. These findings suggest that CHOP, but not caspase-12 or JNK, mainly mediated cardiac apoptosis by proteasome inhibition. Recent research showed that the importance of three ER-initiated apoptotic signals is not equivalently involved in the pathophysiology in ER stress-related diseases.[25–27] Importantly, CHOP knockdown only partially prevented cardiomyocyte death by proteasome inhibition, suggesting that other mechanisms to induce cell death would be involved. Indeed, we have previously demonstrated that proteasome deactivation increased pro-apoptotic regulatory protein levels, such as p53 and Bax, and their knockdown also partially, but significantly, attenuated cardiac apoptosis.[15] These findings suggest that proteasome inhibition may cause cardiac apoptosis via the ER stress-dependent and -independent pathways.

We found overexpression of GRP78 could attenuate both CHOP expression and cell death by proteasome inhibition in cultured cardiomyocytes. In addition, the combination of GRP78 overexpression and CHOP knockdown did not show additional effects on preventing cardiomyocyte death, indicating that cell survival by GRP78 overexpression is predominantly through CHOP-dependent pathway. Further investigation is needed to elucidated why GRP78 specifically blocked CHOP induction among ER-initiated apoptotic signals. In the present study, although CHOP knockdown or GRP78 overexpression showed the small improvement of cell survival when cardiomyocytes were treated with proteasome inhibitors, these findings have some clinical relevance. Since patients will repeatedly receive the proteasome inhibitor for much longer time in the clinical settings, even a small size of improvement will exert the beneficial effects on the patients who need to receive the proteasome inhibitors.

We have previously demonstrated that both CHOP and GRP78 expression were induced in samples from human failing hearts and mouse failing hearts due to the pressure overload.[28] These findings suggest that ER stress may be involved in the pathogenesis in developing heart failure. Although we did not have the opportunity to check the ER-stress related signalling in the animal or human model when proteasome is inhibited, our *in vitro* data strongly suggest that proteasome inhibition may play an important role in the cardiomyocyte death via the ER stress-dependent pathways. The difference in the activation of ER stress-related signalling may be dependent on the pathophysiology of heart failure, and it is necessary to clarify how ER stress is involved in pathogenesis of cardiac diseases.

The ubiquitin-proteasome system is impaired in pathological cardiovascular conditions, such as ischaemia/reperfusion and failing hearts resulting from pressure overload.[15,29] Here, we found that proteasome inhibition induced ER-initiated apoptosis in cultured cardiomyocytes, supporting the idea that the impairment of the ubiquitin-proteasome system may play a crucial role in the development of heart disease. Bortezomib (PS-341) is clinically used as a novel class of anticancer agents against haematological malignancy and solid

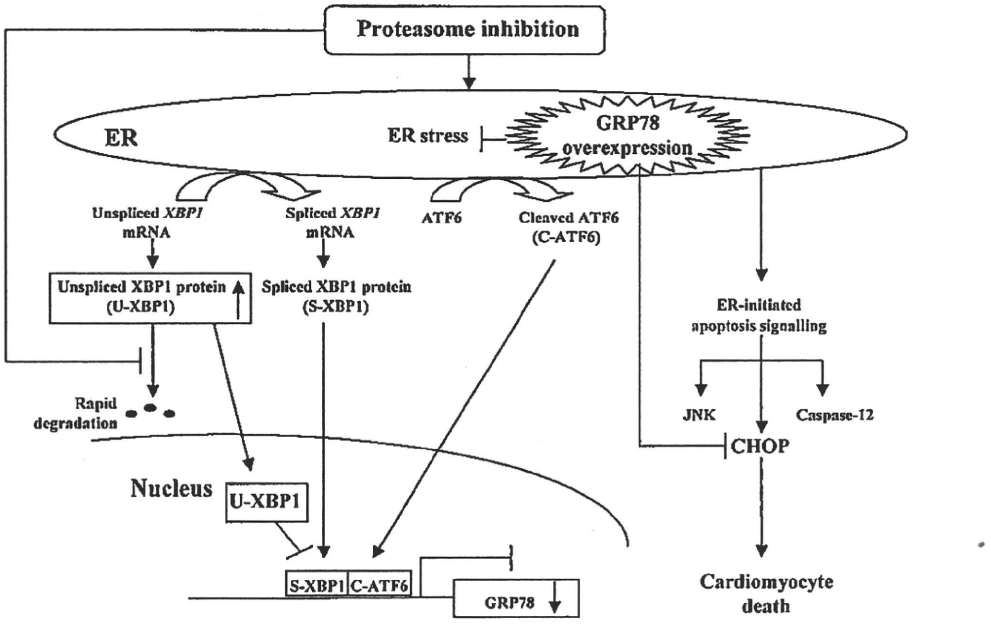

Figure 6 Schematic diagram of endoplasmic reticulum (ER)-chaperone glucose-regulated protein (GRP) 78 attenuating cardiomyocyte death by proteasome inhibition. Proteasome inhibition induces ER stress with the activation of activating transcription factor 6 (ATF6), but not X-box binding protein 1 (XBP1), in cardiomyocytes. Furthermore, proteasome inhibition activates ER-initiated apoptosis signalling such as CCAAT enhancer-binding protein (C/EBP) homologous protein (CHOP), JNK (c-Jun-N-terminal kinase) and caspase-12. Importantly, the expression of GRP78 was not enhanced probably due to the increased protein level of unspliced XBP1, which may further deteriorate ER stress. Overexpression of GRP78 attenuated cardiomyocyte death by proteasome inhibition via CHOP-dependent pathway. U-XBP1, S-XBP1, and C-ATF6 indicate unspliced XBP1, spliced XBP1, and cleaved ATF6, respectively.

tumour. Although bortezomib is not available currently in our hands, MG132 or epoxomicin used in the present study has similar characteristics as bortezomib to cause cell death via ER stress-related signalling.[30,31] Recently, some studies reported that the treatment with bortezomib was associated with cardiac dysfunction.[13,14] In addition, imatinib mesylate, a tyrosine kinase inhibitor used as an anticancer drug, was also reported to cause ER stress and heart failure.[32] Therefore, based on these findings, we need to monitor cardiac function carefully while using anticancer drugs that potentially disrupt protein quality control.

Conflict of interest: none declared.

Funding

This work was supported by a grant for Scientific Research from the Japanese Ministry of Education, Culture, Sports, Science and Technology (No. 17590731) and a grant from Japan Cardiovascular Research Foundation (No. 19390220).

References

1. Kaufman RJ. Stress signaling from the lumen of the endoplasmic reticulum: coordination of gene transcriptional and translational controls. *Genes Dev* 1999;13:1211–1233.
2. Shen J, Chen X, Hendershot L, Prywes R. ER stress regulation of ATF6 localization by dissociation of BIP/GRP78 binding and unmasking of Golgi localization signals. *Dev cell* 2002;3:99–111.
3. Calfon M, Zeng H, Urano F, Till JH, Hubbard SR, Harding HP *et al.* IRE1 couples endoplasmic reticulum load to secretory capacity by processing the XBP-1 mRNA. *Nature* 2002;415:92–96.
4. Yamamoto K, Yoshida H, Kokame K, Kaufman RJ, Mori K. Differential contributions of ATF6 and XBP1 to the activation of endoplasmic reticulum stress-responsive cis-acting elements ERSE, UPRE and ERSE-II. *J Biochem* 2004;136:343–350.
5. Hampton RY. ER-associated degradation in protein quality control and cellular regulation. *Curr Opin Cell Biol* 2002;14:476–482.
6. Oyadomari S, Mori M. Roles of CHOP/GADD153 in endoplasmic reticulum stress. *Cell Death Differ* 2004;11:381–389.
7. Morishima N, Nakanishi K, Takenouchi H, Shibata T, Yasuhiko Y. An endoplasmic reticulum stress-specific caspase cascade in apoptosis. Cytochrome c-independent activation of caspase-9 by caspase-12. *J Biol Chem* 2002;277:34287–34294.
8. Urano F, Wang X, Bertolotti A, Zhang Y, Chung P, Harding HP *et al.* Coupling of stress in the ER to activation of JNK protein kinases by transmembrane protein kinase IRE1. *Science* 2000;287:664–666.
9. Almond JB, Cohen GM. The proteasome: a novel target for cancer chemotherapy. *Leukemia* 2002;16:433–443.
10. Adams J. The development of proteasome inhibitors as anticancer drugs. *Cancer cell* 2004;5:417–421.
11. Kisselev AF, Goldberg AL. Proteasome inhibitors: from research tools to drug candidates. *Chem Biol* 2001;8:739–758.
12. Ludwig H, Khayat D, Giaccone G, Facon T. Proteasome inhibition and its clinical prospects in the treatment of hematologic and solid malignancies. *Cancer* 2005;104:1794–1807.
13. Voortman J, Giaccone G. Severe reversible cardiac failure after bortezomib treatment combined with chemotherapy in a non-small cell lung cancer patient: a case report. *BMC Cancer* 2006;6:129.
14. Enrico O, Gabriele B, Nadia C, Sara G, Daniele V, Giulia C *et al.* Unexpected cardiotoxicity in haematological bortezomib treated patients. *Br J Haemato* 2007;138:396–397.
15. Tsukamoto O, Minamino T, Okada K, Shintani Y, Takashima S, Kato H *et al.* Depression of proteasome activities during the progression of cardiac dysfunction in pressure-overloaded heart of mice. *Biochem Biophys Res Commun* 2006;340:1125–1133.
16. Minamino T, Gaussin V, DeMayo FJ, Schneider MD. Inducible gene targeting in postnatal myocardium by cardiac-specific expression of a hormone-activated Cre fusion protein. *Cir Res* 2001;88:587–592.
17. Shintani Y, Takashima S, Asano Y, Kato H, Liao Y, Yamazaki S *et al.* Glycosaminoglycan modification of neuropilin-1 modulates VEGFR2 signaling. *EMBO J* 2006;25:3045–3055.
18. Thuerauf DJ, Morrison LE, Hoover H, Glembotski CC. Coordination of ATF6-mediated transcription and ATF6 degradation by a domain that is shared with the viral transcription factor, VP16. *J Biol Chem* 2002;277:20734–20739.
19. Lee AH, Iwakoshi NN, Anderson KC, Glimcher LH. Proteasome inhibitors disrupt the unfolded protein response in myeloma cells. *Proc Natl Acad Sci USA* 2003;100:9946–9951.
20. Yoshida H, Matsui T, Yamamoto A, Okada T, Mori K. XBP1 mRNA is induced by ATF6 and spliced by IRE1 in response to ER stress to produce a highly active transcription factor. *Cell* 2001;107:881–891.
21. Li M, Baumeister P, Roy B, Phan T, Foti D, Luo S *et al.* ATF6 as a transcription activator of the endoplasmic reticulum stress element: thapsigargin stress-induced changes and synergistic interactions with NF-Y and YY1. *Mol Cell Biol* 2000;20:5096–5106.
22. Newman JR, Keating AE. Comprehensive identification of human bZIP interactions with coiled-coil arrays. *Science* 2003;300:2097–2101.
23. Yoshida H, Oku M, Suzuki M, Mori K. pXBP1(U) encoded in XBP1 pre-mRNA negatively regulates unfolded protein response activator pXBP1(S) in mammalian ER stress response. *J Cell Biol* 2006;172:565–575.
24. Yamamoto K, Sato T, Matsui T, Sato M, Okada T, Yoshida H *et al.* Transcriptional induction of mammalian ER quality control proteins is mediated by single or combined action of ATF6alpha and XBP1. *Dev Cell* 2007;13:365–376.
25. Kadowaki H, Nishitoh H, Ichijo H. Survival and apoptosis signals in ER stress: the role of protein kinases. *J Chem Neuroanat* 2004;28:93–100.
26. Nakagawa T, Zhu H, Morishima N, Li E, Xu J, Yankner BA *et al.* Caspase-12 mediates endoplasmic-reticulum-specific apoptosis and cytotoxicity by amyloid-beta. *Nature* 2000;403:98–103.
27. Tajiri S, Oyadomari S, Yano S, Morioka M, Gotoh T, Hamada JI *et al.* Ischemia-induced neuronal cell death is mediated by the endoplasmic reticulum stress pathway involving CHOP. *Cell Death Differ* 2004;11:403–415.
28. Okada K, Minamino T, Tsukamoto Y, Liao Y, Tsukamoto O, Takashima S *et al.* Prolonged endoplasmic reticulum stress in hypertrophic and failing heart after aortic constriction: possible contribution of endoplasmic reticulum stress to cardiac myocyte apoptosis. *Circulation* 2004;110:705–712.
29. Kostova Z, Wolf DH. For whom the bell tolls: protein quality control of the endoplasmic reticulum and the ubiquitin-proteasome connection. *EMBO J* 2003;22:2309–2317.
30. Davenport EL, Moore HE, Dunlop AS, Sharp SY, Workman P, Morgan GJ *et al.* Heat shock protein inhibition is associated with activation of the unfolded protein response pathway in myeloma plasma cells. *Blood* 2007;110:2641–2649.
31. Obeng EA, Carlson LM, Gutman DM, Harrington WJ Jr, Lee KP, Boise LH. Proteasome inhibitors induce a terminal unfolded protein response in multiple myeloma cells. *Blood* 2006;107:4907–4916.
32. Kerkela R, Grazette L, Yacobi R, Iliescu C, Patten R, Beahm C *et al.* Cardiotoxicity of the cancer therapeutic agent imatinib mesylate. *Nat Med* 2006;12:908–916.

Journal of the American College of Cardiology
© 2009 by the American College of Cardiology Foundation
Published by Elsevier Inc.

Vol. 53, No. 8, 2009
ISSN 0735-1097/09/$36.00
doi:10.1016/j.jacc.2008.11.014

PRE-CLINICAL RESEARCH

Prolonged Targeting of Ischemic/Reperfused Myocardium by Liposomal Adenosine Augments Cardioprotection in Rats

Hiroyuki Takahama, MD,*†‡ Tetsuo Minamino, MD, PHD,§ Hiroshi Asanuma, MD, PHD,† Masashi Fujita, MD, PHD,§ Tomohiro Asai, PHD,¶ Masakatsu Wakeno, MD, PHD,*†‡ Hideyuki Sasaki, MD,*†‡ Hiroshi Kikuchi, PHD,# Kouichi Hashimoto,** Naoto Oku, PHD,¶ Masanori Asakura, MD, PHD,† Jiyoong Kim, MD,† Seiji Takashima, MD, PHD,§ Kazuo Komamura, MD, PHD,‖ Masaru Sugimachi, MD, PHD,‖ Naoki Mochizuki, MD, PHD,*‡ Masafumi Kitakaze, MD, PHD, FACC†

Osaka, Shizuoka, and Tokyo, Japan

Objectives The purpose of this study was to investigate whether liposomal adenosine has stronger cardioprotective effects and fewer side effects than free adenosine.

Background Liposomes are nanoparticles that can deliver various agents to target tissues and delay degradation of these agents. Liposomes coated with polyethylene glycol (PEG) prolong the residence time of drugs in the blood. Although adenosine reduces the myocardial infarct (MI) size in clinical trials, it also causes hypotension and bradycardia.

Methods We prepared PEGylated liposomal adenosine (mean diameter 134 ± 21 nm) by the hydration method. In rats, we evaluated the myocardial accumulation of liposomes and MI size at 3 h after 30 min of ischemia followed by reperfusion.

Results The electron microscopy and ex vivo bioluminescence imaging showed the specific accumulation of liposomes in ischemic/reperfused myocardium. Investigation of radioisotope-labeled adenosine encapsulated in PEGylated liposomes revealed a prolonged blood residence time. An intravenous infusion of PEGylated liposomal adenosine (450 μg/kg/min) had a weaker effect on blood pressure and heart rate than the corresponding dose of free adenosine. An intravenous infusion of PEGylated liposomal adenosine (450 μg/kg/min) for 10 min from 5 min before the onset of reperfusion significantly reduced MI size (29.5 ± 6.5%) compared with an infusion of saline (53.2 ± 3.5%, $p < 0.05$). The antagonist of adenosine A_1, A_{2a}, A_{2b}, or A_3 subtype receptor blocked cardioprotection observed in the PEGylated liposomal adenosine-treated group.

Conclusions An infusion as PEGylated liposomes augmented the cardioprotective effects of adenosine against ischemia/reperfusion injury and reduced its unfavorable hemodynamic effects. Liposomes are promising for developing new treatments for acute MI. (J Am Coll Cardiol 2009;53:709–17) © 2009 by the American College of Cardiology Foundation

Liposomes are now widely used for drug delivery in cancer treatment to target specific organs actively or passively and to prevent the degradation of chemotherapy agents (1). However, the application of liposomes for cardiovascular diseases is still limited. In ischemic/reperfused myocardium,

See page 718

cellular permeability is enhanced and vascular endothelial integrity is disrupted (2,3), suggesting that nanoparticles

*From the Department of Molecular Imaging in Cardiovascular Medicine, Osaka University Graduate School of Medicine, Osaka, Japan; †Department of Cardiovascular Medicine, National Cardiovascular Center, Osaka, Japan; ‡Department of Structural Analysis, Research Institute, National Cardiovascular Center, Osaka, Japan; §Department of Cardiovascular Medicine, Osaka University Graduate School of Medicine, Osaka, Japan; ‖Department of Cardiovascular Dynamics, Research Institute, National Cardiovascular Center, Osaka, Japan; ¶Department of Medical Biochemistry, School of Pharmaceutical Sciences, University of Shizuoka, Shizuoka, Japan; #Daiichi Pharmaceutical Co., Tokyo, Japan; and the **Daiichi-Sankyo Pharmaceutical Co., Tokyo, Japan. Supported by a grant for Scientific Research and a grant for the Advancement of Medical Equipment from the Japanese Ministry of Health, Labor, and Welfare, as well as a grant from the Japan Cardiovascular Research Foundation.

Manuscript received September 4, 2008; revised manuscript received October 21, 2008, accepted November 3, 2008.

Abbreviations and Acronyms

8-SPT = 8-(p-sulfophenyl) theophylline
EM = electron microscopy
MI = myocardial infarction
PEG = polyethylene glycol
RI = radioisotope
TTC = triphenyltetrazolium chloride

such as liposomes may be a promising drug delivery system for targeting damaged myocardium with cardioprotective agents. Additionally, coating liposomes with polyethylene glycol (PEG) prolongs their residence time in the circulation (1). Because enhanced microvascular permeability persists for at least 48 h after the occurrence of myocardial infarction (MI) (2), drugs delivered in PEGylated liposomes should be able to display their maximum beneficial effects on myocardial damage after MI.

Adenosine has multiple physiological functions that are mediated via the adenosine A_1, A_{2a}, A_{2b}, and A_3 receptors (4,5). Although large-scale clinical trials suggested the potential value of adenosine therapy for patients with acute MI (6,7), this agent has an extremely short half-life (1 to 2 s) and causes hypotension and bradycardia because of vasodilatory and negative chronotropic effects (4). Because a high dose of adenosine is required to exert cardioprotective effects, it is difficult to use clinically because of the associated hemodynamic consequences. Therefore, we hypothesized that adenosine encapsulated in PEGylated liposomes would cause less hemodynamic disturbance and might also specifically accumulate in ischemic/reperfused myocardium, leading to augmented cardioprotective effects. To test this hypothesis, we created PEGylated liposomal adenosine by the hydration method and investigated: 1) whether liposomal adenosine accumulated in ischemic/reperfused myocardium and prolonged blood residence time; 2) whether liposomal adenosine caused less severe hypotension and bradycardia than free adenosine; and 3) which adenosine receptor subtype was involved in mediating the cardioprotective effects of liposomal adenosine against ischemia/reperfusion injury.

Methods

Materials. The materials for preparing PEGylated liposomes, including hydrogenated soy phosphatidyl choline (HSPC), 1,2-distearoyl-sn-glycero-3-phosphoethanolamine-n-[methoxy (polyethylene glycol)-2000] (DSPE-PEG2000), and cholesterol were obtained from Nissei Oil Co., Ltd. (Tokyo, Japan) and Wako Pure Chemical Co., Ltd. (Osaka, Japan). [^{3}H]-adenosine was purchased from Daiichi Pure Chemicals Co., Ltd. (Tokyo, Japan). Other materials were obtained from Sigma (St. Louis, Missouri), including 8-(*p*-sulfophenyl)theophylline (8-SPT; a nonselective adenosine receptor antagonist), 1,3-diethyl-8-phenylxanthine (DPCPX; a selective adenosine A_1 receptor antagonist), 5-amino-7-(phenylethyl)-2-(2-furyl)-pyrazolo[4,3-e]-1,2,4-triazolo[1,5-c] pyrimidine (SCH58261; a selective adenosine A_{2a} receptor antagonist), 8-[4-[((4-cyanophenyl)carbamoylmethyl) oxy]phenyl]-1, 3-di(n-propyl)xanthine (MRS1754; a selective adenosine A_{2b} receptor antagonist), and 5-propyl-2-ethyl-4-propyl-3-(ethylsulfanylcarbonyl)-6-phenylpyridine-5-carboxylate (MRS1523, a selective adenosine A_3 receptor antagonist).

Animals. Male Wistar rats (9 weeks old and weighing 250 to 310 g, Japan Animals, Osaka, Japan) were used. The animal experiments were approved by the National Cardiovascular Center Research Committee and were performed according to institutional guidelines.

Preparation of PEGylated liposomes. The PEGylated liposomes were prepared by the hydration method. Briefly, adenosine was added to the lipid solution. After mixture of lipid and adenosine, DSPE-PEG2000 was added and incubated. The final composition of PEGylated liposomes was HSPC:cholesterol:DSPE-PEG2000 = 6.0:4.0:0.3 (molar ratio). After ultracentrifugation several times, the pellet of liposomal adenosine was resuspended in sodium lactate at each required concentration for use in the experimental protocols. Some samples of final liposomal adenosine were disrupted by dilution with 50% methanol (1.5 ml per 30-μl of liposomes). After 10 min of ultracentrifugation, the concentration of adenosine in the supernatant was measured by high-performance liquid chromatography.

To prepare fluorescent-labeled liposomes, 0.5 mol% tetramethylrhodamine isothiocyanate (rhodamine) was added to the lipid mixture. To prepare radioisotope (RI)-labeled adenosine encapsulated in liposomes, [^{3}H]-radiolabeled adenosine (Daiichi Pure Chemicals, Tokyo, Japan) was diluted with free adenosine and was encapsulated in liposomes as described above.

Characterization of PEGylated liposomal adenosine. The characterization of the liposomes was performed by the dynamic scatter analysis (Zetasizer Nano ZS, Malvern, Worcestershire, United Kingdom). The analyses were performed 10 times per sample, and results represented analyses of 4 independent experiments.

Experimental protocols. PROTOCOL 1: EFFECTS OF PEGYLATED LIPOSOMAL ADENOSINE ON HEMODYNAMICS IN RATS. Rats were anesthetized with intraperitoneal sodium pentobarbital (50 mg/kg). Catheters were advanced into a femoral artery and vein for the measurement of systemic blood pressure and infusion of drugs, respectively. Both blood pressure and heart rate were monitored continuously during the study using a Power Lab (AD Instruments, Castle Hill, Australia). After hemodynamics became stable, we intravenously administered empty PEGylated liposomes (n = 8), free adenosine (n = 8), or PEGylated liposomal adenosine (n = 8) for 10 min. Either PEGylated liposomal or free adenosine was infused at an initial dose of 225 μg/kg/min (0.1 ml/min) for 10 min. After a 5-min interval, either PEGylated liposomal adenosine or free adenosine was infused at 450 μg/kg/min (0.1 ml/min) for 10 min. In the same manner, PEGylated liposomal adenosine or free adenosine was then infused at 900 μg/kg/min (0.1 ml/min).

PROTOCOL 2: EFFECTS OF PEGYLATED LIPOSOMAL ADENOSINE ON INFARCT SIZE IN RATS. The MI was induced by transient ligation of the left coronary artery as described previously (8). In the first series of experiments, to examine the dose-dependent effects of liposomal adenosine on MI size, PEGylated liposomal adenosine was infused intravenously at 50, 150, or 450 μg/kg/min for a 10-min period starting from 5 min before the onset of reperfusion. In the second series of experiments, to determine the adenosine receptor subtype involved in cardioprotective effects by the liposomal adenosine, the antagonist of adenosine subtype receptor was intravenously injected as a bolus followed by the infusion of liposomal adenosine for 10 min. The MI size was evaluated at 3 h after the start of reperfusion. The doses of adenosine receptor subtype antagonists were determined according to the previous reports (9–11).

Measurement of infarct size. At 3 h after the onset of reperfusion, the area at risk and the infarcted area were determined by Evans blue and triphenyltetrazolium chloride (TTC) staining, respectively, as previously described (8). Infarct size was calculated as [infarcted area/area at risk] × 100(%) in a blind manner. The area at risk was composed of border (TTC staining) and infarcted (TTC nonstaining) areas.

Electron microscopy (EM). Myocardial samples for EM were obtained from the central and peripheral areas in ischemic/reperfused myocardium, which roughly corresponded to the infarcted and border areas, respectively, after the left coronary artery was occluded for 30 min of ischemia followed by 3 h of reperfusion. Samples were prepared as previously reported (12). Liposomes, whose major membrane component is unsaturated phospholipids, were visualized as homogenous dark dots with a diameter of 100 to 150 nm (13).

Accumulation of fluorescent-labeled PEGylated liposomes in ischemic/reperfused myocardium. Unlabeled or fluorescent-labeled PEGylated liposomes were infused intravenously at a dose of 0.1 ml/min as liposomal adenosine was infused in protocol 2. At 3 h after reperfusion, hearts were quickly removed and cut into 4 sections parallel to the axis from base to apex. Then ex vivo bioluminescence imaging was performed with an Olympus OV 100 imaging system (Olympus, Tokyo, Japan) and signals were quantified using WASABI quantitative software (Hamamatsu Photonics K.K., Shizuoka, Japan). Fluorescent intensity in the region of interest was measured as previously reported (14). Control intensity indicated the fluorescent intensity in the nonischemic area of the individual rat.

Time-course changes of free and PEGylated liposomal RI-labeled adenosine in plasma and myocardium. Free or PEGylated liposomal [^{3}H]-adenosine (83 kBq per rat) was infused intravenously at a dose of 0.1 ml/min as liposomal adenosine was infused in protocol 2. At the time indicated, rat hearts were harvested for counting of radioactivity (LSC-3100, Aloka Co., Tokyo, Japan). Results are expressed as a percentage of the injected dose per 1 ml of blood or 1 g of wet tissue weight.

Statistical analysis. The parameters of the liposomes were expressed as the average ± SD, whereas other data were expressed as the average ± SEM. Comparison of time-course changes in hemodynamic parameters between groups was performed by 2-way repeated-measures analysis of variance (ANOVA) followed by a post-hoc Bonferroni test. For comparison of RI activity between groups, statistical analysis was done with the Mann-Whitney *U* test. To address the differences in infarct size among groups, we performed a nonparametric (Kruskal-Wallis) test followed by evaluation with the Mann-Whitney *U* test. Resulting p values were corrected according to the Bonferroni method. To compare parameters of liposomes, an unpaired *t* test was performed. In all analyses, $p < 0.05$ was considered to indicate statistical significance.

Results

Characterization of liposomes by dynamic light scatter analysis. The dynamic light scatter analysis showed no significant difference in mean diameter, polydispersity index, or zeta-potential distribution between empty and adenosine-loaded PEGylated liposomes (Table 1).

Liposomes in ischemic/reperfused myocardium. The EM revealed the intact vascular endothelial cells and cardiomyocytes in the nonischemic myocardium (Figs. 1A and 1B). There were no homogenous dark dots indicating liposomes in the nonischemic myocardium of rats that received either saline (Fig. 1A) or liposomes (Fig. 1B). In the border area, many homogenous dark dots indicating liposomes were accumulated in rats that received liposomes, but not saline (Figs. 1C and 1D). In this area, significant structural damage was not observed in endothelium, but slight swelling of mitochondria was often observed. In the infarcted area, numerous liposomes were detected in rats that received liposomes, but not saline (Figs. 1E and 1F). In this area, the disrupted endothelial integrity and marked swelling of mitochondria were often observed.

Table 1 Characterization of Liposomes by Dynamic Light Scatter Analysis

	Mean Diameter (nm)	Polydispersity Index	Zeta Potential (mV)
PEGylated liposomes (empty liposomes)	126 ± 12	0.035 ± 0.003	−1.7 ± 0.4
PEGylated liposomal adenosine	134 ± 21	0.094 ± 0.002	−2.3 ± 1.1

Results represented analysis of 4 independent experiments. Values are expressed as mean ± SD.
PEG = polyethylene glycol.

JACC Vol. 53, No. 8, 2009
February 24, 2009:709–17

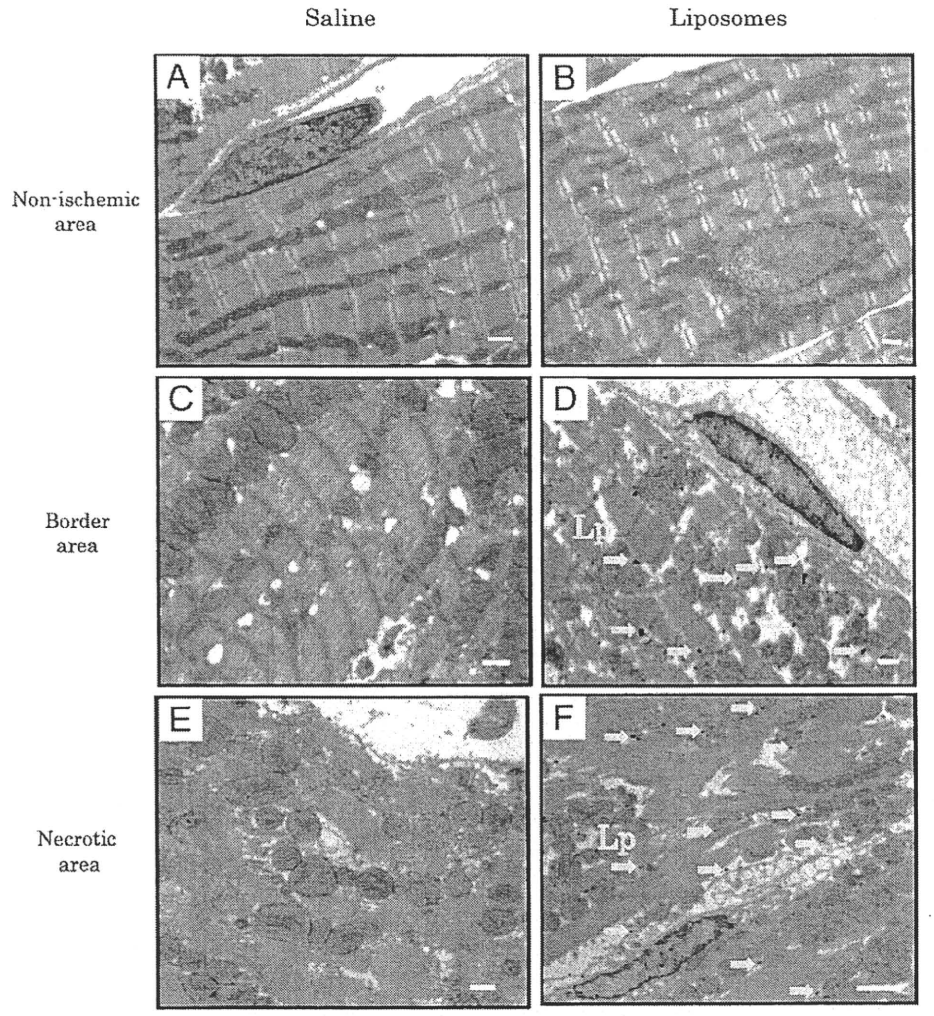

Figure 1 Liposomes in Ischemic/Reperfused Myocardium

(A, B) Representative electron micrographs of the nonischemic area in rats that received saline **(A)** or liposomes (Lp) **(B)**. **(C, D)** Representative electron micrographs of border area at 3 h after myocardial infarction (MI). Many **dark dots** accumulated in this area in the rat that received liposomes but not saline. **(E, F)** Representative electron micrographs of infarcted areas at 3 h after MI. Numerous **dark dots** accumulated in this area in the rat that received liposomes but not saline. Scale bars represent 1 μm.

Fluorescent-labeled PEGylated liposomes in ischemic/reperfused myocardium. Quantitative analysis by bioluminescence ex vivo bioluminescene imaging revealed that the target to control fluorescent intensity ratio was higher in the border (noninfarcted area at risk) as well as infarcted areas compared with a nonischemic one, suggesting that fluorescent-labeled liposomes were accumulated in the border as well as infarcted areas. Since there was no high-intensity area when unlabeled liposomes were infused, it was suggested that this was not a nonspecific phenomenon to MI by the ex vivo bioluminescence imaging system (Fig. 2). The Evans blue staining was unrelated to the fluorescence intensity (data not shown).

Plasma radioactivity of RI-labeled adenosine was markedly higher in the PEGylated liposomal adenosine group at 10 min and 3 h after the intravenous infusion than in the free adenosine group (Fig. 3A). Encapsulation within PEGylated liposomes also augmented the accumulation of adenosine in ischemic/reperfused myocardium compared with that of free adenosine (Fig. 3B).

Hemodynamic effects of PEGylated liposomal adenosine. Baseline hemodynamic parameters did not differ among the groups. An intravenous infusion of free adenosine at doses of 225, 450, and 900 μg/kg/min decreased the mean blood pressure by 14.8%, 25.4%, and 33.7%, respectively, compared with the effect of empty PEGylated lipo-

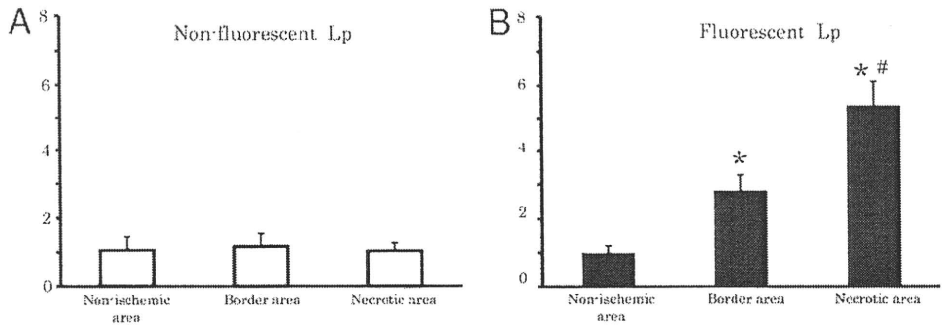

Figure 2 **Detection of Fluorescence-Labeled PEGylated Liposomes in Ischemic/Reperfused Myocardium**

Quantitative analysis of target-to-control fluorescent intensity ratio for each area in rats (n = 3 each group) that received nonfluorescent **(A)** or fluorescent **(B)** liposomes. The values of bioluminescence signals in the border and infarcted areas were expressed as the fold to that of the each nonischemic area. Values are expressed as the mean ± SEM (error bars). *p < 0.05 versus nonischemic areas. #p < 0.05 versus border areas.

somes. In contrast, the intravenous infusion of PEGylated liposomal adenosine at a dose of either 225 or 450 μg/kg/min did not significantly alter mean blood pressure (Fig. 4). Changes of the heart rate after infusion of PEGylated liposomal adenosine or free adenosine were similar to those observed for mean blood pressure (Fig. 4).

Effects of PEGylated liposomal adenosine on MI size. Baseline hemodynamic parameters were similar among all of the groups (Table 2). Intravenous infusion of free adenosine for 10 min reduced both the blood pressure and the heart rate, although these parameters returned to baseline within 5 min of ceasing infusion (Table 2). In contrast, hemodynamic parameters of the other groups were not altered (Table 2). The area at risk in the control group (61 ± 3%) did not differ compared with those of other groups that received liposomal adenosine. Intravenous infusion of PEGylated liposomal adenosine caused a dose-dependent decrease of MI size compared with that in the control group, whereas intravenous infusion of empty PEGylated liposomes or free adenosine did not (Fig. 5B).

The bolus injection of adenosine receptor antagonist did not alter the hemodynamic parameters (Table 3). The area at risk in the liposomal adenosine group (58 ± 3%) did not differ compared with those of other groups that received adenosine receptor antagonist. Infusion of 8-SPT, a nonspecific adenosine receptor antagonist, blunted the cardioprotective effect of liposomal adenosine (Fig. 6B). Furthermore, the infusion of the adenosine A_1, A_{2a}, A_{2b}, or A_3 receptor antagonist also blunted cardioprotective effects of liposomal adenosine (Fig. 6B). Infusion of 8-SPT alone did not significantly affect myocardial infarct size compared with the control (52 ± 5%, n = 4).

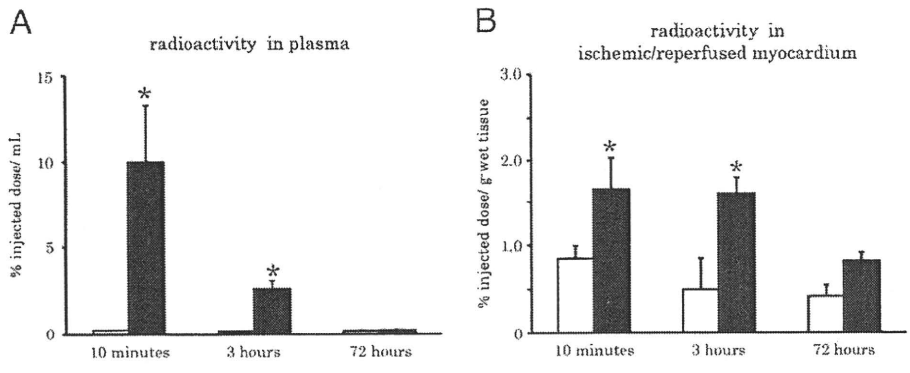

Figure 3 **Radioisotope-Labeled Adenosine in Plasma and Ischemic/Reperfused Myocardium**

(A) Changes in plasma radioactivity after infusion of radioisotope-labeled adenosine. **Solid and open bars** indicate the PEGylated liposomal adenosine and free adenosine groups, respectively (n = 4 each). In the PEGylated liposomal adenosine group, plasma radioactivity was markedly higher than in the free adenosine group. **(B)** Changes in radioactivity in ischemic/reperfused myocardium. **Solid and open bars** indicate the PEGylated liposomal adenosine and free adenosine groups, respectively (n = 4 each). In the PEGylated liposomal adenosine group, myocardial radioactivity was markedly higher than in the free adenosine group. Values are expressed as the mean ± SEM (error bars). *p < 0.05 versus the free adenosine group at the corresponding time.

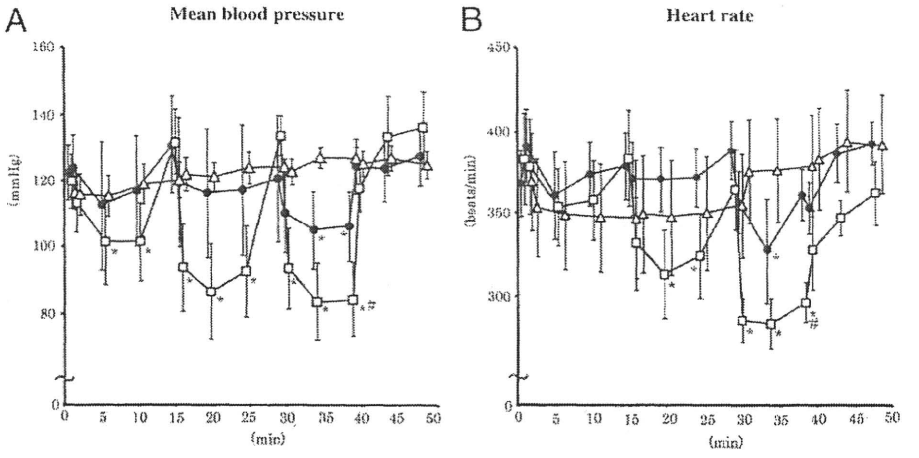

Figure 4 **Hemodynamic Effects of PEGylated Liposomal Adenosine**

Changes in the mean blood pressure **(A)** and heart rate **(B)** after intravenous infusion of various doses of empty PEGylated liposomes **(triangles)**, PEGylated liposomal adenosine **(circles)**, or free adenosine **(squares)** (n = 8 each). Values are expressed as the mean ± SEM. *p < 0.05 versus baseline at the corresponding group. #p < 0.05 versus PEGylated liposomes.

Discussion

In the present study, EM, bioluminescence ex vivo imaging, and fluorescent analysis revealed the accumulation of liposomes in the border (noninfarcted areas at risk) as well as infarcted ones, but not nonischemic myocardium, at 3 h after MI. These findings suggested that liposomes could specifically accumulate in ischemic/reperfused myocardium. Interestingly, EM revealed the existence of liposomes at sites where endothelial integrity was still morphologically maintained. Endothelial dysfunction such as enhanced permeability is induced by ischemic insult without morphological endothelial disruption (3,15). Enhanced permeability might lead to the accumulation of liposomes in the border as well as infarcted area, which will contribute to salvage the ischemic/reperfused myocardium. However, further investigation will be needed to determine the precise mechanism by which liposomes accumulate in ischemic/reperfused myocardium.

Analysis using RI-labeled adenosine encapsulated in liposomes revealed that plasma radioactivity was markedly higher in the PEGylated liposomal adenosine group compared with the free adenosine group. This indicates that encapsulation of adenosine by PEGylated liposomes considerably prolonged its residence time in the circulation and delayed its degradation. Consistent with the histological data, RI-labeled adenosine also showed preferential accumulation in ischemic/reperfused myocardium.

Table 2 **Effects of Liposomal Adenosine on Hemodynamic Parameters**

		Ischemia				Reperfusion	
	Baseline	0 min	15 min	25 min	30 min	5 min	10 min
Mean blood pressure (mm Hg)							
Saline	122 ± 5	102 ± 10	108 ± 7	107 ± 9	108 ± 7	105 ± 9	104 ± 9
Vehicle	127 ± 4	109 ± 8	108 ± 7	111 ± 9	111 ± 5	105 ± 5	103 ± 5
Free-Ado	124 ± 8	115 ± 8	111 ± 5	109 ± 4	66 ± 4*	62 ± 4*	112 ± 6
Lp-Ado 50 μg/kg/min	121 ± 5	106 ± 6	105 ± 6	110 ± 10	102 ± 6	101 ± 6	104 ± 4
Lp-Ado 150 μg/kg/min	122 ± 3	107 ± 6	107 ± 6	109 ± 11	105 ± 6	100 ± 6	103 ± 4
Lp-Ado 450 μg/kg/min	124 ± 3	104 ± 6	105 ± 6	107 ± 5	102 ± 6	99 ± 6	104 ± 4
Heart rate (beats/min)							
Saline	363 ± 22	366 ± 19	369 ± 14	413 ± 22	372 ± 12	372 ± 16	371 ± 14
Vehicle	363 ± 32	363 ± 6	383 ± 6	396 ± 25	367 ± 6	374 ± 7	372 ± 7
Free-Ado	360 ± 18	361 ± 17	384 ± 13	379 ± 18	305 ± 11*	293 ± 13*	356 ± 14
Lp-Ado 50 μg/kg/min	378 ± 19	386 ± 21	366 ± 12	376 ± 12	367 ± 19	369 ± 9	377 ± 17
Lp-Ado 150 μg/kg/min	388 ± 27	376 ± 20	371 ± 14	377 ± 13	378 ± 16	373 ± 16	369 ± 17
Lp-Ado 450 μg/kg/min	368 ± 17	376 ± 21	361 ± 13	386 ± 15	368 ± 15	363 ± 6	367 ± 7

Values are expressed as mean ± SEM. *p < 0.05 versus baseline.
Free-Ado = free adenosine; Lp-Ado = PEGylated liposomal adenosine; PEG = polyethylene glycol; vehicle = PEGylated liposomes.

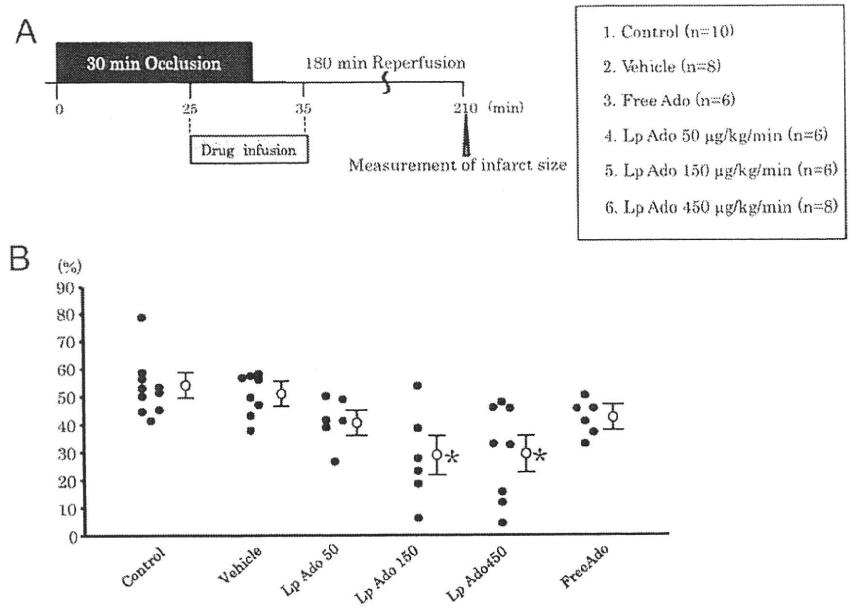

Figure 5 **Dose-Dependent Effects of PEGylated Liposomal Adenosine on Myocardial Infarct Size**

(A) Protocol showing the timing of infusion of PEGylated liposomal adenosine and of infarct size measurement. **(B)** Myocardial infarct size. Values are expressed as mean ± SEM (error bars). *$p < 0.05$ versus the control group. Free-Ado = free adenosine; Lp-Ado = PEGylated liposomal adenosine; Vehicle = PEGylated liposomes.

Furthermore, this study showed that PEGylated liposomal adenosine had a weaker effect on the blood pressure and heart rate than free adenosine. Thus, encapsulating adenosine in PEGylated liposomes attenuated its vasodilatory and negative chronotropic effects, presumably by reducing the amount of circulating free adenosine. However, the changes of hemodynamic parameters in this in vivo model suggested that significant release of adenosine from PEGylated liposomes would still occur if a large dose of liposomal adenosine (e.g., 900 μg/kg/min) were administered. Thus, further investigation of the in vivo pharmacodynamics of PEGylated liposomal adenosine is needed.

An intravenous infusion of PEGylated liposomal adenosine at the maximum dose that did not disturb hemodynamic parameters for 10 min before reperfusion reduced MI size in a dose-dependent manner, and this improvement was blocked by 8-SPT, a nonselective adenosine receptor antagonist. These findings suggest that adenosine released from liposomes acts via an adenosine receptor-dependent pathway. One possible mechanism by which PEGylated lipo-

Table 3 **Effects of Adenosine Receptor Antagonist on Hemodynamic Parameters**

		Ischemia				Reperfusion	
	Baseline	0 min	15 min	25 min	30 min	5 min	10 min
Mean blood pressure (mm Hg)							
Lp-Ado + 8SPT	120 ± 6	113 ± 4	112 ± 6	112 ± 5	107 ± 6	102 ± 8	109 ± 7
Lp-Ado + DPCPX	130 ± 6	105 ± 4	121 ± 4	100 ± 10	122 ± 6	120 ± 6	111 ± 4
Lp-Ado + SCH58261	132 ± 2	98 ± 12	99 ± 8	110 ± 8	118 ± 10	113 ± 10	109 ± 6
Lp-Ado + MRS1754	130 ± 3	95 ± 12	106 ± 8	105 ± 10	100 ± 10	96 ± 10	99 ± 7
Lp-Ado + MRS1523	130 ± 2	109 ± 8	104 ± 8	105 ± 9	100 ± 9	101 ± 10	104 ± 6
Heart rate (beats/min)							
Lp-Ado + 8SPT	404 ± 17	385 ± 10	374 ± 8	396 ± 8	389 ± 9	383 ± 8	385 ± 9
Lp-Ado + DPCPX	396 ± 24	380 ± 11	399 ± 9	398 ± 12	385 ± 9	382 ± 9	380 ± 7
Lp-Ado + SCH58261	393 ± 14	399 ± 15	381 ± 9	395 ± 15	376 ± 9	373 ± 9	385 ± 7
Lp-Ado + MRS1754	398 ± 14	392 ± 11	401 ± 9	379 ± 15	378 ± 9	374 ± 9	377 ± 7
Lp-Ado + MRS1523	396 ± 9	390 ± 11	390 ± 11	392 ± 10	373 ± 9	391 ± 7	388 ± 11

Values were expressed as mean ± SEM. *$p < 0.05$ versus baseline.
Lp-Ado = PEGylated liposomal adenosine; PEG = polyethylene glycol; Vehicle = PEGylated liposomes.

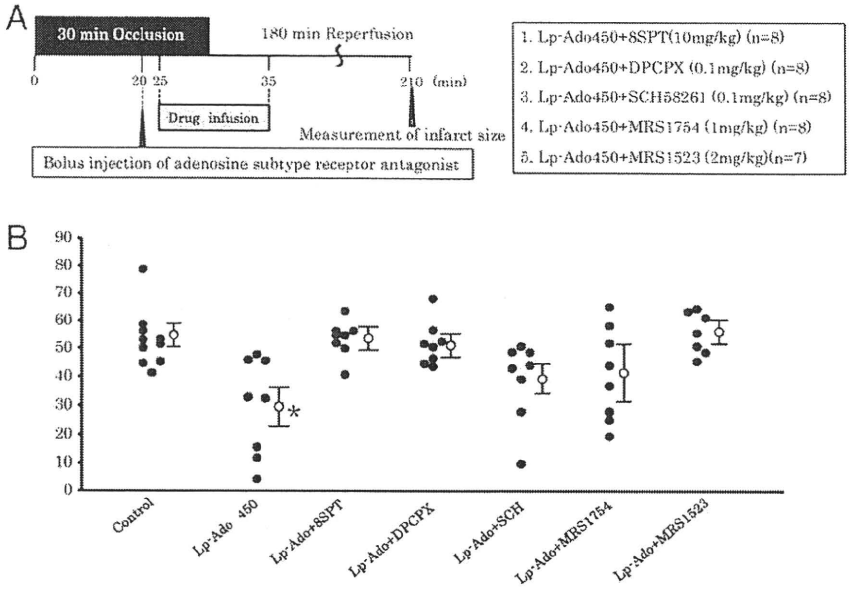

Figure 6 **Effects of Adenosine Receptor Antagonists on Myocardial Infarct Size**

(A) Protocol showing the timing of infusion of PEGylated liposomal adenosine and bolus injection adenosine receptor antagonists. **(B)** Myocardial infarct size. Values are expressed as the mean ± SEM (error bars). *$p < 0.05$ versus the control group. The abbreviations for adenosine antagonists were described in the text. Abbreviations as in Figure 5.

somes could augment cardioprotective effects of liposomal adenosine with minimum effects on hemodynamic parameters is the enhanced accumulation of PEGylated liposomal adenosine in ischemic/reperfused myocardium, which could augment various beneficial actions such as preventing calcium overload in the myocardium (5). The prolonged persistence of PEGylated liposomal adenosine would also increase its beneficial effect on ischemic/reperfused myocardium. Although continuous high-dose, long-term infusion of free adenosine was reported to reduce infarct size in rats (16), the present study did not confirm such a cardioprotective effect, probably because the total dose of free adenosine that we used was not high enough.

We found that myocardial infarct size in the group that received PEGylated liposomal adenosine with the antagonist of adenosine A_1, A_{2a}, A_{2b}, or A_3 subtype receptor was no different from the control group, indicating that every adenosine subtype receptor could possibly play a role in mediating cardioprotection by liposomal adenosine and that it was difficult to identify one particular subtype in the present study. Numerous studies reported that A_1, A_{2a}, A_{2b}, and A_3 receptors have been involved in cardioprotection against ischemia/reperfusion injury, and it remains controversial which adenosine subtype receptor is most responsible for cardioprotection (17–20). Furthermore, because the adenosine receptor antagonists used in the present study had some nonspecific effects, future investigation will be needed to examine the precise role of each adenosine receptor subtype using genetically engineered mice.

Because liposomal adenosine infused during reperfusion could reduce MI size, this agent could be a candidate for the adjunctive therapy of patients with acute MI. Importantly, adenosine is currently used for the diagnosis of ischemic heart disease and PEGylated liposomes are used to deliver anticancer agents (21). Thus, it should not be difficult to introduce PEGylated liposomal adenosine into clinical practice. Finally, PEGylated liposomes may provide a useful drug delivery system for targeting ischemic/reperfused myocardium with other agents.

Acknowledgments

The authors thank Akiko Ogai and Yoko Nakano for their excellent technical assistance; Motohide Takahama, Hiroyuki Hao, and Hatsue Ishibashi-Ueda for advice about the electron microscopy figure; and Syunichi Kuroda and Takashi Matsuzaki for assistance with bioluminescence imaging.

Reprint requests and correspondence: Dr. Tetsuo Minamino, Department of Cardiovascular Medicine, Osaka University Graduate School of Medicine, 2-2 Yamadaoka, Suita, Osaka 565-0871, Japan. E-mail: minamino@medone.med.osaka-u.ac.jp.

REFERENCES

1. Papahadjopoulos D, Allen TM, Gabizon A, et al. Sterically stabilized liposomes: improvements in pharmacokinetics and antitumor therapeutic efficacy. Proc Natl Acad Sci U S A 1991;24:11460–4.

2. Horwitz LD, Kaufman D, Keller MW, Kong Y. Time course of coronary endothelial healing after injury due to ischemia and reperfusion. Circulation 1994;90:2439–47.
3. Dauber IM, Van Benthuysen KM, McMurtry IF, et al. Functional coronary microvascular injury evident as increased permeability due to brief ischemia and reperfusion. Circ Res 1990;66:986–98.
4. Forman MB, Stone GW, Jackson EK. Role of adenosine as adjunctive therapy in acute myocardial infarction. Cardiovasc Drug Rev 2006;24: 116–47.
5. Mubagwa K, Flameng W. Adenosine, adenosine receptors and myocardial protection: an updated overview. Cardiovasc Res 2001;52:25–39.
6. Mahaffey KW, Pune JA, Barbagelata NA, et al. Adenosine as an adjunct to thrombolytic therapy for acute myocardial infarction: results of a multicenter, randomized, placebo-controlled trial: the Acute Myocardial Infarction STudy of ADenosine (AMISTAD) trial. J Am Coll Cardiol 1999;34:1711–20.
7. Ross AM, Gibbons RJ, Stone GW, Kloner RA, Alexander RW, for the AMISTAD-II AInvestigators. A randomized, double-blinded, placebo-controlled multicenter trial of adenosine as an adjunct to reperfusion in the treatment of acute myocardial infarction (AMISTAD-II). J Am Coll Cardiol 2005;45:1775–80.
8. Bullard AJ, Govewalla P, Yellon DM. Erythropoietin protects the myocardium against reperfusion injury in vitro and in vivo. Basic Res Cardiol 2005;100:397–403.
9. Hannon JP, Tigani B, Wolber C, et al. Evidence for an atypical receptor mediating the augmented bronchoconstrictor response to adenosine induced by allergen challenge in activity sensitized Brown Norway rats. Br J Pharmacol 2002;135:685–96.
10. Kin H, Zatta AJ, Lofye MT, et al. Postconditioning reduces infarct size via adenosine receptor activation by endogenous adenosine. Cardiovasc Res 2005;67:124–33.
11. Hinschen AK, RoseMeyer RB, Headrick JP. Adenosine receptor subtypes mediating coronary vasodilation in rat hearts. J Cardiovasc Pharmacol 2003;41:73–80.
12. Kaeffeer N, Richard V, Francois A, Lallemand F, Henry JP, Thuillez C. Preconditioning prevents chronic reperfusion-induced coronary endothelial dysfunction in rats. Am J Physiol 1996;271:H842–9.
13. M Shimizu, Miwa K, Hashimoto Y, Goto A. Encapsulating of chicken egg yolk immunoglobulin G (IgY) by liposomes. Biosci Biotechnol Biochem 1993;57:1445–9.
14. Kasuya T, Jung J, Kadoya H, et al. In vivo delivery of bionanocapsules displaying phaseolus vulgaris agglutinin-L(4) isolectin to malignant tumors overexpressing N-acetylglucosaminlyltransferase V. Hum Gene Ther 2008;19:887–95.
15. Kim YD, Fomsgaard JS, Heim KF, et al. Brief ischemia-reperfusion induces stunning of endothelium in canine coronary artery. Circulation 1992;85:1473–82.
16. Canyon SJ, Dobson GP. Protection against ventricular arrhythmias and cardiac death using adenosine and lidocaine during regional ischemia in the in vivo rat. Am J Physiol Heart Circ Physiol 2004;287:H1286–95.
17. Yaar R, Jones MR, Chen JF, Ravid K. Animal models for the study of adenosineÂreceptor function. J Cell Physiol 2005;202:9–20.
18. Norton ED, Jackson EK, Turner MB, Virmani R, Forman MB. The effects of intravenous infusions of selective adenosine A_1-receptor and A_2-receptor agonists on myocardial reperfusion injury. Am Heart J 1992;123:332–8.
19. Xu Z, Mueller RA, Park SS, Boysen PG, Cohen MV, Downey JM. Cardioprotection with adenosine A_2 receptor activation at reperfusion. J Cardiovasc Pharmacol 2005;46:794–802.
20. Vinten-Johansen J. Postconditioning: a mechanical maneuver that triggers biological and molecular cardioprotective responses to reperfusion. Heart Fail Rev 2007;12:235–344.
21. Lasic DD. Doxorubicin in sterically stabilized liposomes. Nature 1996;380:561–2.

Key Words: myocardial infarction ▪ liposome ▪ drug delivery system ▪ adenosine.

JACC: CARDIOVASCULAR IMAGING
© 2009 BY THE AMERICAN COLLEGE OF CARDIOLOGY FOUNDATION
PUBLISHED BY ELSEVIER INC.

VOL. 2, NO. 6, 2009
ISSN 1936-878X/09/$36.00
DOI:10.1016/j.jcmg.2008.11.019

Heterogeneous Onset of Myocardial Relaxation in Subendocardial and Subepicardial Layers Assessed With Tissue Strain Imaging

Comparison of Normal and Hypertrophied Myocardium

Takuya Hasegawa, MD,* Satoshi Nakatani, MD,† Hideaki Kanzaki, MD,*
Haruhiko Abe, MD,* Masafumi Kitakaze, MD*
Osaka, Japan

OBJECTIVES We sought to investigate the existence of a time difference in myocardial relaxation between the subendocardium and subepicardium in patients with and without myocardial hypertrophy.

BACKGROUND Regional differences in mechanical and electrical properties between the subendocardium and subepicardium have been described for the left ventricle in animals. However, this difference has not been well evaluated in clinical conditions.

METHODS Time-to-peak radial strain with reference to the QRS complex was measured at the subendocardium and subepicardium at the mid-posterior wall of the left ventricle in 12 normal subjects, 14 patients with hypertensive heart disease, and 27 patients with aortic stenosis (16 with and 11 without strain electrocardiogram [ECG] pattern) using tissue Doppler-based strain imaging.

RESULTS Time-to-peak radial strain in the subepicardium (381 ± 60 ms) was shorter than that in the subendocardium (463 ± 29 ms; $p < 0.001$) in normal subjects, suggesting that the subepicardial relaxation precedes subendocardial relaxation. No significant difference was found between normal subjects and patients with hypertensive heart disease (388 ± 67 ms for the subepicardium; 455 ± 36 ms for the subendocardium in hypertensive heart disease). In cases with hypertrophied myocardium due to aortic stenosis, time-to-peak radial strain in the subendocardium was shortened and that in the subepicardium was prolonged. In 10 (63%) of 16 patients with aortic stenosis and strain ECG pattern, the timing of peak strain in the subendocardium (417 ± 63 ms) preceded that in the subepicardium (452 ± 62 ms).

CONCLUSIONS There is heterogeneous onset of myocardial relaxation in the subendocardial and subepicardial layers at the mid-posterior wall of the left ventricle. Subepicardial myocardial relaxation precedes subendocardial relaxation in normal subjects. In contrast, there is inversion of the transmural sequence of myocardial relaxation between the subendocardium and subepicardium in some patients with aortic stenosis and strain ECG pattern. (J Am Coll Cardiol Img 2009;2:701–8) © 2009 by the American College of Cardiology Foundation

From the *Department of Cardiology, National Cardiovascular Center, Osaka, Japan; and the †Division of Functional Diagnostics, Department of Health Sciences, Osaka University Graduate School of Medicine, Osaka, Japan.

Manuscript received June 19, 2008; revised manuscript received November 6, 2008, accepted November 16, 2008.

JACC: CARDIOVASCULAR IMAGING, VOL. 2, NO. 6, 2009
JUNE 2009:701–8

Transmural heterogeneity of the onset of myocardial contraction and relaxation has been observed in normal animal hearts using sonomicrometry and magnetic resonance imaging, and in an in vitro study using isolated myocytes (1–4). In the normal myocardium, the time-to-peak cell shortening is longer in the subendocardium than in the subepicardium. This time difference has also been described in an in vitro study using isolated myocytes with hypertrophied guinea pig hearts (3). In that study, the time difference to peak cell shortening between the subendocardium and subepicardium was less in hypertrophied myocardium than in normal myocardium. However, transmural mechanics has yet to be investigated in human hearts, and transmural mechanics in hypertrophied myocardium has not been described under clinical conditions. Investigation of transmural mechanics with a noninvasive method would provide important basic and clinical relevance concerning the pathophysiology of various myocardial diseases.

ABBREVIATIONS AND ACRONYMS

AS-NT = aortic stenosis without strain T on electrocardiogram
AS-ST = aortic stenosis with strain T on electrocardiogram
AVC = aortic valve closure
ECG = electrocardiogram
HT = hypertensive heart disease
LV = left ventricular
N = normal subjects
TP-ε = time-to-peak radial strain

Tissue Doppler imaging enables us to measure change in regional myocardial length noninvasively over the complete cardiac cycle. With the recent development of myocardial strain imaging obtained by tissue Doppler imaging, we can estimate regional myocardial thickening over an entire cardiac cycle without being affected by cardiac translation and assess transmural distribution of myocardial strain (5). In the present study, we used myocardial strain imaging to determine whether the time difference to peak myocardial thickening between the subendocardium and subepicardium was observed in normal and hypertrophied human hearts.

METHODS

Study patients. The study subjects consisted of 27 patients with left ventricular (LV) hypertrophy caused by severe aortic stenosis, 14 patients with LV hypertrophy and a history of hypertension (Group HT), and 12 normal subjects (Group N). The subjects in Groups HT and N had no symptoms or echocardiographic findings suggestive of any cardiovascular disease other than hypertension. The patients with severe aortic stenosis were divided into 2 groups: 11 patients without strain T on electrocardiogram (ECG) (Group AS-NT) and 16 patients with strain T (Group AS-ST). Strain T was defined as asymmetric ST depression in any lead except aVR, and V_1 to V_3 in the absence of bundle-branch block. No significant coronary artery lesions were demonstrated by coronary angiography in any of patients with aortic stenosis. This study was conducted in accordance with institutional ethical guidelines, and all patients gave written, informed consent.

Standard echocardiography. Standard echocardiography and color tissue Doppler imaging were performed using a commercially available ultrasound scanner with a 2.5-MHz transducer (Aplio, Toshiba Medical Systems, Tokyo, Japan). The LV dimension, wall thickness, and transmitral inflow pattern were measured according to the guidelines of the American Society of Echocardiography (6). The LV ejection fraction was calculated using the Quinones formula (7). The LV mass was calculated using the Devereux formula (8). The severity of aortic stenosis was assessed by peak aortic valve pressure gradient and aortic valve area calculated using the continuity equation (9).

Tissue strain imaging. The LV short-axis image at the mid-level was obtained by color tissue Doppler imaging with a frame rate of 60 to 80 Hz and was analyzed offline using commercially available software (TDI-Q, Toshiba Medical Systems, Tokyo, Japan).

TDI-Q software enables accurate evaluation of regional myocardial strain using 2 novel techniques: the tissue Doppler tracking technique (5,10–12) and the angle-correction technique (5,12). Briefly, with the tissue Doppler tracking technique, motion of an arbitrary point on the myocardium is tracked during a cardiac cycle, based on the myocardial velocity information as follows (10). By integrating the velocity of an indexed point on the ventricular wall known from tissue Doppler imaging, we can obtain myocardial displacement and predict where the point will move next. By repeating this procedure, the system automatically tracks the motion of the point. The influence of myocardial translation can be neglected using this technique.

The angle-correction technique has been used to partly overcome the Doppler angle dependency that has been described in previous reports (5,12). To correct the Doppler incident angle, a contraction center is manually set at the center of the LV cavity in the LV short-axis view at end-systole. The myocardial velocity toward the contraction center (V motion) is automatically calculated by dividing the velocity toward the transducer (V beam) by the

cosine of the angle (θ) between the Doppler beam and the direction to the contraction center:

$$V \text{ motion} = V \text{ beam}/\cos \theta$$

Using these 2 techniques, TDI-Q provides myocardial velocity, and displacement and strain as a result of velocity integration toward the contraction center without being affected by myocardial translation or the Doppler incident angle (5,10,11). In a previous experiment, the displacement data obtained by this method correlated well with true displacement ($r = 0.99$, $p < 0.0001$) (11).

Strain is defined as the change in distance between 2 myocardial points divided by the initial length (L_0). In clinical studies with echocardiography, myocardial strain is calculated using the following equation:

$$(L - L_0)/L_0$$

where L is the instantaneous length (13). In the present study, the distance of all 2-pixel pairs at end-diastole (equivalent to L_0) was set at 2 mm. Using the tissue tracking technique, we can obtain the displacement of the 2 points in the subendocardium or the subepicardium toward the contraction center. Therefore, we can obtain myocardial radial strain in the subendocardium and subepicardium separately in a cardiac cycle.

Measurement of time-to-peak strain. Figure 1 shows the temporal changes in myocardial radial strain in the subendocardium and subepicardium at the mid-LV posterior wall using TDI-Q. In the present study, subendocardium was defined as the inner one-third of the LV myocardium, and subepicardium was defined as the outer one-third of the LV myocardium. The myocardium contracts until myocardial radial strain reaches a peak, after which it relaxes.

We measured time-to-peak radial strain (TP-ε) in the subendocardium and subepicardium at the mid-LV posterior wall with reference to the onset of QRS on ECG and calculated the difference of TP-ε between the layers. TP-ε was divided by the time to aortic valve closure (AVC) from the onset of QRS on ECG to correct for differences in heart rate (TP-ε/AVC). Time to AVC was measured using pulsed-wave Doppler echocardiography of the LV outflow.

Statistical analysis. Data were expressed as mean ± SD. Comparison of the parameters of clinical characteristics and echocardiography among the groups

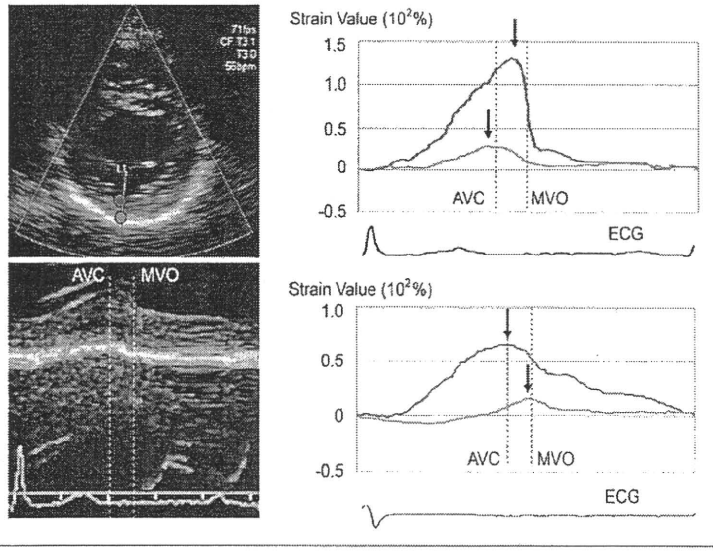

Figure 1. Temporal Myocardial Radial Strain Profile of the Subendocardium and Subepicardium in a Normal Subject and a Subject With Aortic Stenosis and Strain ECG Pattern

The **upper left panel** shows a left ventricular short-axis image from a parasternal approach at end-diastole in a normal subject. The **red dot** is on the subendocardium, and the **orange dot** is on the subepicardium. The **lower left panel** shows M-mode imaging of the mid-left ventricular posterior region in the normal subject. The **upper right panel** shows temporal radial strain profile at the mid-left ventricular posterior region in the normal subject. The **red curve in the lower panel** shows the myocardial strain profile in the subendocardium; the **orange curve** shows that in the subepicardium. The **lower right panel** shows temporal radial strain profile in a subject with aortic stenosis and strain ECG pattern. The arrows indicate the peak myocardial strain in each layer. AVC = aortic valve closure; ECG = electrocardiogram; MVO = mitral valve closure.

JACC: CARDIOVASCULAR IMAGING, VOL. 2, NO. 6, 2009
JUNE 2009:701–8

was performed using one-way analysis of variance followed by Fisher multiple comparison tests. Categorical data among the groups were compared using the Pearson chi-square test. Unpaired Student *t* testing was used to compare the severity of aortic stenosis between patients with and without strain T and to compare the difference in TP-ε between the subendocardium and subepicardium. A p value of <0.05 was considered statistically significant. All statistical analyses were performed using Stat View 5.0 for Windows (SAS Institute, Cary, North Carolina).

TP-ε was measured by 2 independent observers and by 1 observer twice, a week apart, in 10 randomly selected segments to determine inter- and intraobserver variability. Variability was expressed as the absolute difference between the 2 measurements as a percentage of their mean values. Interobserver and intraobserver variability for TP-ε were 5.6 ± 6.4% and 4.8 ± 6.9%, respectively.

RESULTS

Clinical and echocardiographic characteristics. The characteristics of the patients are shown in Table 1. There was no significant difference in age and gender among the patients and normal subjects.

Left ventricular contraction was preserved, and LV wall motion abnormality was not observed in any patients. The LV wall thickness and LV mass of patients in Group AS-NT were similar to those in Group HT. The LV wall was thicker in patients in Group AS-ST than those in Group AS-NT ($p < 0.01$). Doppler parameters of transmitral inflow suggested that diastolic function was similar among all groups, although patients in Group AS-ST had higher late diastolic inflow than those in the other groups ($p < 0.05$). In patients with aortic stenosis, aortic valve pressure gradient was significantly higher in patients in Group AS-ST than in those in Group AS-NT.

Time-to-peak radial strain in the subendocardium and subepicardium. Figure 2 shows the difference in TP-ε among the 4 groups. Although LV hypertrophy was observed in patients in Group HT, TP-ε in Group HT was similar to that of Group N in both the subendocardium and subepicardium. However, TP-ε in the subendocardium was shorter ($p < 0.05$) in patients with aortic stenosis than that in normal subjects, suggesting that subendocardial re-

Table 1. Patient Characteristics and Data of Standard Echocardiography

Variables	N (n = 12)	HT (n = 14)	AS-NT (n = 11)	AS-ST (n = 16)	p Value
Patient characteristics					
Age, yrs	61 ± 13	64 ± 12	63 ± 11	67 ± 13	0.620
Male, n (%)	7 (58)	9 (64)	6 (55)	7 (44)	0.716
Systolic blood pressure, mm Hg	127 ± 17	136 ± 13	124 ± 16	119 ± 16†	0.043
Diastolic blood pressure, mm Hg	75 ± 9	79 ± 13	67 ± 6†	66 ± 9†	0.002
Heart rate, beats/min	63 ± 12	63 ± 13	64 ± 13	65 ± 10	0.949
Standard echocardiography					
LV end-diastolic diameter, mm	48 ± 4	44 ± 4	46 ± 4	42 ± 5*	0.008
LV end-systolic diameter, mm	29 ± 5	27 ± 5	27 ± 2	26 ± 5	0.186
Ejection fraction, %	73 ± 7	72 ± 7	75 ± 6	73 ± 7	0.761
Thickness of IVS, mm	9 ± 1	12 ± 1*	13 ± 1*	14 ± 2*†‡	<0.001
Thickness of PW, mm	9 ± 1	12 ± 1*	12 ± 2*	14 ± 2*†‡	<0.001
LV mass, g	145 ± 33	186 ± 35	216 ± 55*	227 ± 47*	<0.001
Mitral Doppler inflow					
E-wave, cm/s	70 ± 17	67 ± 14	58 ± 15	76 ± 20	0.061
A-wave, cm/s	76 ± 22	81 ± 22	80 ± 13	103 ± 31*	0.011
E/A	0.99 ± 0.40	0.88 ± 0.28	0.75 ± 0.29	0.78 ± 0.27	0.222
Deceleration time of E-wave, ms	225 ± 23	263 ± 68	260 ± 72	258 ± 131	0.674
The severity of aortic stenosis					
Peak pressure gradient, mm Hg	n/a	n/a	87 ± 36	120 ± 38	0.036
Aortic valve area, cm^2	n/a	n/a	0.72 ± 0.32	0.54 ± 0.14	0.056

*$p < 0.05$ versus Group N; †$p < 0.05$ versus Group HT; ‡$p < 0.05$ versus Group AS-NT.
AS-NT = aortic stenosis without strain T ECG; AS-ST = aortic stenosis with strain T ECG; HT = hypertensive heart disease; IVS = intraventricular septal wall; LV = left ventricular; N = normal subjects; PW = posterior wall.

laxation at the mid-LV posterior wall occurs earlier in patients with aortic stenosis than in normal subjects. TP-ε in the subepicardium was longer in Group AS-ST (452 ± 62 ms, $p < 0.05$) than in the other groups.

Figure 3 shows a comparison of TP-ε/AVC among the 4 groups. For subjects in Group N and Group HT, TP-ε/AVC in the subendocardium was greater than 1.0 (1.063 ± 0.050 and 1.079 ± 0.116, respectively), whereas that in the subepicardium was less than 1.0 (0.876 ± 0.140 and 0.913 ± 0.121, respectively). This indicates that myocardial relaxation in the subepicardium occurred before AVC, and that myocardial relaxation in the subendocardium occurred after AVC at the mid-LV posterior wall. Interestingly, this sequence was different in patients with aortic stenosis: subendocardial relaxation occurred before AVC in 18 of 27 patients with aortic stenosis. Subepicardial relaxation occurred after AVC in 9 of 16 patients with aortic stenosis and ECG strain pattern.

Transmural sequence of myocardial relaxation. We calculated the difference in TP-ε between the subendocardium and subepicardium to investigate transmural discordance of myocardial relaxation at the mid-LV posterior wall (Fig. 4). In normal subjects, the timing of peak radial strain in the subepicardium (381 ± 60 ms) preceded that in the subendocardium (463 ± 29 ms, $p < 0.001$), indicating that myocardial relaxation at the mid-LV posterior wall occurred in the subepicardium before that in the subendocardium by about 80 ms.

In Group AS-ST, because TP-ε in the subendocardium (452 ± 62 ms, $p < 0.05$) was shorter and that in the subepicardium (417 ± 63 ms, $p < 0.05$) was longer than those in Group N and Group HT, the difference in TP-ε between the subendocardium and subepicardium (−35 ± 74 ms) was significantly shorter than that in Group N and Group HT (82 ± 45 ms and 67 ± 62 ms, respectively). In 10 (63%) of 16 patients with severe aortic stenosis and ECG strain T-wave, the difference was negative, indicating inversion of the transmural sequence of myocardial relaxation.

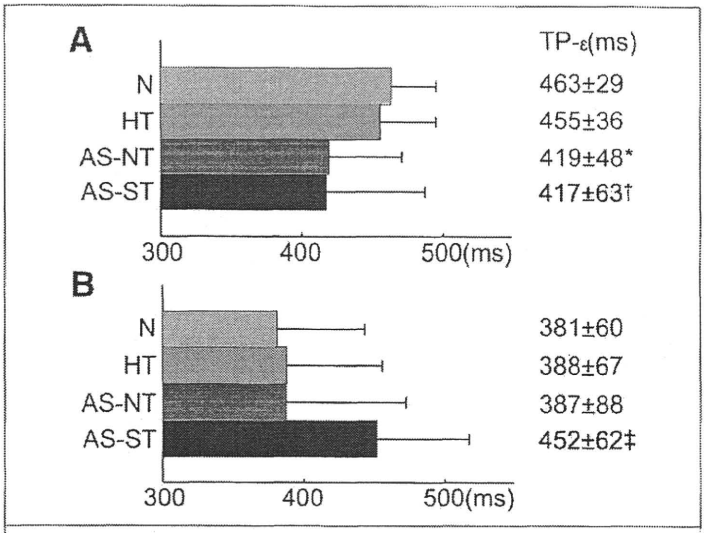

Figure 2. TP-ε in the Subendocardium and Subepicardium

Time-to-peak radial strain in the subendocardium (A) and subepicardium (B). *$p < 0.05$ versus Group N (normal subjects); †$p < 0.05$ versus Group N and Group HT (patients with hypertensive heart disease); ‡$p < 0.05$ versus the other groups. AS-NT = aortic stenosis without strain T on electrocardiogram; AS-ST = aortic stenosis with strain T on electrocardiogram; TP-ε = time-to-peak strain from the onset of QRS on electrocardiogram; other abbreviations as in Figure 1.

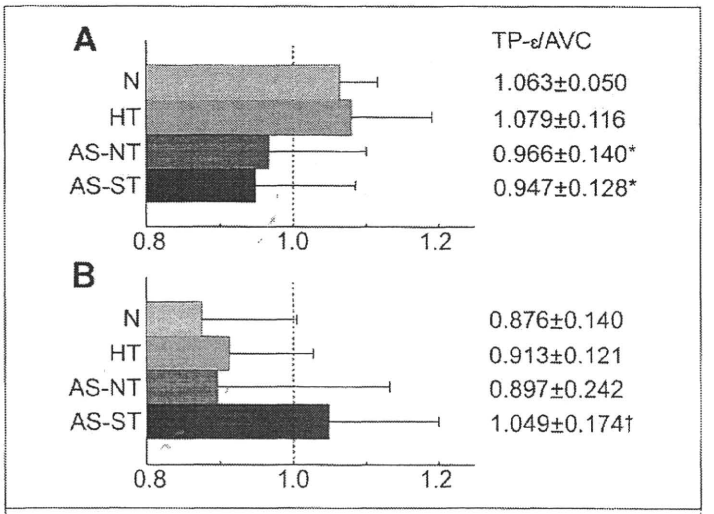

Figure 3. Ratio of TP-ε to Time to AVC

Time-to-peak radial strain /AVC in the subendocardium (A) and subepicardium (B). If the TP-ε/AVC ratio is greater than 1.0, the timing of strain peak is located beyond that of AVC. *$p < 0.05$ versus Group N and Group HT; †$p < 0.05$ versus other groups. TP-ε/AVC = ratio of TP-ε to time to AVC from the onset of QRS on ECG; other abbreviations as in Figures 1 and 2.

DISCUSSION

We demonstrated myocardial radial strain profile and transmural mechanics at the mid-LV posterior wall in humans using echocardiography for the first time. Our results indicate that in normal subjects the onset of myocardial relaxation in the subepicardium precedes that in the subendocardium at the mid-LV posterior wall, and that the transmural sequence is inverted in some patients with severely hypertrophied hearts.

JACC: CARDIOVASCULAR IMAGING, VOL. 2, NO. 6, 2009
JUNE 2009:701–8

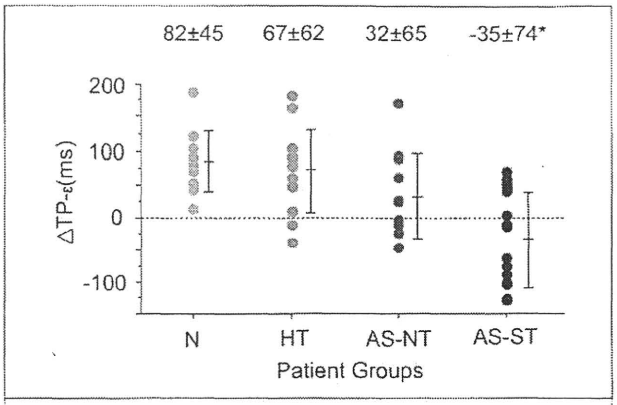

Figure 4. Difference in TP-ε Between the Subendocardium and the Subepicardium

The negative value for Group AS-ST indicates that the timing of strain peak in the subendocardium precedes that in the subepicardium at the mid-left ventricular posterior region. *$p < 0.01$ versus all other groups. Abbreviations as in Figure 2.

Transmural mechanics assessed by echocardiography in normal human hearts. We demonstrated that the onset of subepicardial relaxation precedes subendocardial relaxation at the mid-LV posterior wall in normal human hearts. The transmural heterogeneity of myocardial strain value in human hearts has been described previously using magnetic resonance imaging (14). However, the transmural sequence of myocardial relaxation has not been previously investigated in human hearts. The transmural sequence has been studied in normal animal hearts using sonomicrometry and in isolated myocytes (1–3); these results are consistent with our data of normal human hearts assessed by echocardiography.

We also found that subendocardial contraction at the mid-LV posterior wall sustained after AVC. During isovolumic relaxation, apical untwisting is accompanied by relaxation and expansion of LV apex (1). This generates a rapid base-to-apex reversal of isovolumic intracavitary pressure and blood flow (15,16). Because volume cannot change within isovolumic relaxation, subendocardial wall thickening at the basal to middle region might sustain after AVC with the apical expansion.

Transmural mechanics assessed by echocardiography in hypertrophied hearts. We also demonstrated differences in the transmural sequence of myocardial relaxation between normal and severely hypertrophied left ventricles at the mid-LV posterior region. There was no significant difference in the transmural sequence of myocardial relaxation between Group N and Group HT, indicating that wall thickness itself may not be a major determinant of transmural difference in relaxation timing. However, the onset of subendocardial relaxation in Group AS-NT was earlier than that in Group HT. Although previous studies indicate that high LV pressure appears to affect myocardial strain value and LV segmental dyssynchrony (17,18), its effect on time-to-peak strain in the subendocardium has not been studied. The high LV pressure in end-systole may depress thickening of the subendocardium in patients with aortic stenosis resulting in a shortened duration of thickening.

The onset of subepicardial relaxation was delayed in Group AS-ST, compared with patients in Group AS-NT, and the transmural sequence of relaxation was inverted in some patients. It is known that transmural electrical heterogeneity exists in the myocardium and affects the ECG waveform (19). There are 3 types of gradient that are responsible for genesis of T-wave: 1) differences between the right and left ventricle; 2) differences between apex-base and anterior-posterior walls; and 3) transmural difference (20). In previous investigations, the presence of a repolarization gradient between the "mid-myocardial region" (M-cells) and subendocardial and subepicardial regions has been correlated with the genesis of upright T waves in ventricular wedge preparations (21). However, studies of intact hearts have failed to provide evidence for transmural differences in repolarization (22). Thus, the genesis of T-wave on surface ECG may be largely due to the base-to-apex gradient with minimum contribution from the transmural gradient (1). The presence of strain T-wave may be accompanied with significant change of the electrical property in the myocardial cells in the whole left ventricle, which generates not only base-to-apex gradient but also the transmural gradient to some extent in the hypertrophied hearts. Actually, a previous in vitro study (3) found that the action potential duration in the subepicardium and midcardium becomes longer as LV hypertrophy progresses, and that the time-to-peak cell shortening also becomes longer. In contrast, the action potential duration in the subendocardium becomes shorter and the time-to-peak cell shortening becomes shorter, although the degree is an insignificant amount. In the present study, we found that the onset of myocardial relaxation in the subendocardium and subepicardium at the mid-LV posterior wall was almost coincident, and that in some patients the onset of subendocardial relaxation preceded that of subepicardial relaxation. These findings are consistent with those of the earlier animal study (3).

Clinical implications. The present study is the first report regarding the transmural mechanics in normal and hypertrophied myocardium under clinical conditions. There are a lot of conditions with T-wave alteration such as myocardial hypertrophy, ischemia, and cardiac arrhythmias including the Brugada syndrome and long QT syndrome. We believe that our present method should be useful to investigate transmural electromechanical sequence of relaxation, and also contraction, and could provide new insights into the pathophysiology of these conditions.

We demonstrated the difference in the onset of myocardial relaxation between the subendocardium and subepicardium using echocardiography, without opening the chest and implanting crystals, as has been performed in some reports that focused on transmural mechanics using sonomicrometry with open-chest animals (1,2). The invasive method cannot be applied to humans. Moreover, the implantation of the crystals may cause local scarring and induce abnormal wall motion not only due to the implantation procedure, but also due to their weight and inertial properties. The thoracotomy itself can alter the temperature of the epicardial surface and change its action potential duration and T-wave polarity (23). Opening the pericardium could affect the whole cardiac motion and regional myocardial deformation. In contrast, the recent development of echocardiography has enabled the investigation of the transmural myocardial deformation in clinical settings (5,10–12).

We assumed that earlier myocardial relaxation of the subepicardium might facilitate the following relaxation of the subendocardium so that the early LV filling occurs efficiently. However, unfortunately, in this study, we could not find a significant association of the difference in TP-e between the subendocardium and subepicardium with transmitral E-wave velocity ($r = 0.011$, $p = 0.940$). Further study will be needed using more sophisticated indexes of LV filling or relaxation.

Study limitations. In the present study, we assessed myocardial strain only at the mid-posterior wall; therefore, our results may not apply to the other LV segments. Our findings may not relate to aortic stenosis, but may reflect the consequences of LV pressure load. We did not measure actual LV pressure when we obtained the echocardiographic data. The LV pressure and wall stress affect the myocardial strain profile. The difference in the onset of myocardial relaxation among the 4 groups may be caused by differences in the hemodynamic condition rather than differences in electrical properties, especially in the subendocardium. Despite these limitations, we consider that our method is a successful noninvasive technique for demonstrating the transmural sequence of myocardial relaxation.

We set the initial length to obtain instantaneous radial strain at 2 mm. A longer length would be advantageous for obtaining peak radial strain but a smaller length would be better for obtaining regional information. In the present study, we measured time-to-peak strain, which might be less affected by noise than peak strain even with a smaller initial length.

CONCLUSIONS

Myocardial relaxation of the subepicardium precedes that of the subendocardium at the mid-LV posterior wall in the normal human myocardium. In the hypertrophied myocardium with aortic stenosis, the onset of myocardial relaxation in the subendocardium is earlier than that in normal myocardium at the mid-LV posterior wall, whereas the onset in the subepicardium is later than that in the normal myocardium. In some patients with severe hypertrophy and strain T-wave, there is an inversion of the transmural sequence of the myocardial relaxation, compared with that in normal subjects.

Reprint requests and correspondence: Dr. Satoshi Nakatani, Division of Functional Diagnostics, Department of Health Sciences, Osaka University Graduate School of Medicine, 1-7 Yamada-oka, Suita, Osaka 565-0871, Japan. *E-mail: nakatani@sahs.med.osaka-u.ac.jp.*

REFERENCES

1. Sengupta PP, Khandheria BK, Korinek J, et al. Apex-to-base dispersion in regional timing of left ventricular shortening and lengthening. J Am Coll Cardiol 2006;47:163–72.
2. Ashikaga H, Coppola BA, Hopenfeld B, et al. Transmural dispersion of myofiber mechanics: implications for electrical heterogeneity in vivo. J Am Coll Cardiol 2007;49:909–16.
3. Bryant SM, Shipsey SJ, Hart G. Regional differences in electrical and mechanical properties of myocytes from guinea-pig hearts with mild left ventricular hypertrophy. Cardiovasc Res 1997;35:315–23.
4. Ashikaga H, Mickelsen SR, Ennis DB, et al. Electromechanical analysis of infarct border zone in chronic myocardial infarction. Am J Physiol Heart Circ Physiol 2005;289:H1099–105.

5. Maruo T, Nakatani S, Jin Y, et al. Evaluation of transmural distribution of viable muscle by myocardial strain profile and dobutamine stress echocardiography. Am J Physiol Heart Circ Physiol 2007;292:H921–7.
6. Lang RM, Bierig M, Devereux RB, et al., on behalf of Chamber Quantification Writing Group, American Society of Echocardiography's Guidelines and Standards Committee, European Association of Echocardiography. Recommendations for chamber quantification: a report from the American Society of Echocardiography's Guidelines and Standards Committee and the Chamber Quantification Writing Group, developed in conjunction with the European Association of Echocardiography, a branch of the European Society of Cardiology. J Am Soc Echocardiogr 2005;18:1440–63.
7. Quinones MA, Waggoner AD, Reduto LA, et al. A new, simplified and accurate method for determining ejection fraction with two-dimensional echocardiography. Circulation 1981;64:744–53.
8. Devereux RB, Alonso DR, Lutas EM, et al. Echocardiographic assessment of left ventricular hypertrophy: comparison to necropsy findings. Am J Cardiol 1986;57:450–8.
9. Quinones MA, Otto CM, Stoddard M, et al., on behalf of Doppler Quantification Task Force of the Nomenclature and Standards Committee of the American Society of Echocardiography. Recommendations for quantification of Doppler echocardiography: a report from the Doppler Quantification Task Force of the Nomenclature and Standards Committee of the American Society of Echocardiography. J Am Soc Echocardiogr 2002;15:167–84.
10. Tanaka N, Tonc T, Ono S, et al. Predominant inner-half wall thickening of left ventricle is attenuated in dilated cardiomyopathy: an application of tissue Doppler tracking technique. J Am Soc Echocardiogr 2001;14:97–103.
11. Sade LE, Severyn DA, Kanzaki H, et al. Second-generation tissue Doppler with angle-corrected color-coded wall displacement for quantitative assessment of regional left ventricular function. Am J Cardiol 2003;92:554–60.
12. Dohi K, Pinsky MR, Kanzaki H, et al. Effects of radial left ventricular dyssynchrony on cardiac performance using quantitative tissue Doppler radial strain imaging. J Am Soc Echocardiogr 2006;19:475–82.
13. Urheim S, Edvardsen T, Torp H, et al. Myocardial strain by Doppler echocardiography. Validation of a new method to quantify regional myocardial function. Circulation 2000;102:1158–64.
14. Bogaert J, Rademakers FE. Regional nonuniformity of normal adult human left ventricle. Am J Physiol Heart Circ Physiol 2001;280:H610–20.
15. Goetz WA, Lansac E, Lim HS, et al. Left ventricular endocardial longitudinal and transverse changes during isovolumic contraction and relaxation: a challenge. Am J Physiol Heart Circ Physiol 2005;289:H196–201.
16. Sengupta PP, Khandheria BK, Korinek J, et al. Left ventricular isovolumic flow sequence during sinus and paced rhythms: new insights from use of high-resolution Doppler and ultrasonic digital particle imaging velocimetry. J Am Coll Cardiol 2007;49:899–908.
17. Biederman RW, Doyle M, Yamrozik J, et al. Physiologic compensation is supranormal in compensated aortic stenosis: does it return to normal after aortic valve replacement or is it blunted by coexistent coronary artery disease? An intramyocardial magnetic resonance imaging study. Circulation 2005;112:I429–36.
18. Park TH, Lakkis NM, Middleton KJ, et al. Acute effect of nonsurgical septal reduction therapy on regional left ventricular asynchrony in patients with hypertrophic obstructive cardiomyopathy. Circulation 2002;106:412–5.
19. Wilson FN, Macleod AG, Barker PS, Johnston FD. The determination and the significance of the areas of the ventricular deflections of the electrocardiogram. Am Heart J 1934;10:46–61.
20. Opthof T. In vivo dispersion in repolarization and arrhythmias in the human heart. Am J Physiol Heart Circ Physiol 2006;290:H77–8.
21. Antzelevitch C. Transmural dispersion of repolarization and the T wave. Cardiovasc Res 2001;50:426–31.
22. Janse MJ, Sosunov EA, Coronel R, et al. Repolarization gradients in the canine left ventricle before and after induction of short-term cardiac memory. Circulation. 2005;112:1711–8.
23. Inoue M, Hori M, Kajiya F, et al. Theoretical analysis of T-wave polarity based on a model of cardiac electrical activity. J Electrocardiol 1978;11:171–80.

Key Words: echocardiography ■ hypertrophy ■ electrocardiography.

Journal of the American College of Cardiology
© 2009 by the American College of Cardiology Foundation
Published by Elsevier Inc.

Vol. 53, No. 22, 2009
ISSN 0735-1097/09/$36.00
doi:10.1016/j.jacc.2009.02.038

Natriuretic Peptides Enhance the Production of Adiponectin in Human Adipocytes and in Patients With Chronic Heart Failure

Osamu Tsukamoto, MD, PHD,*‡ Masashi Fujita, MD, PHD,‡ Mahoto Kato, MD,* Satoru Yamazaki, PHD,* Yoshihiro Asano, MD, PHD,‡ Akiko Ogai, PHD,* Hidetoshi Okazaki, MD, PHD,* Mitsutoshi Asai, MD,‡ Yoko Nagamachi, BS,‡ Norikazu Maeda, MD, PHD,§ Yasunori Shintani, MD, PHD,‡ Tetsuo Minamino, MD, PHD,‡ Masanori Asakura, MD, PHD,* Ichiro Kishimoto, MD, PHD,† Tohru Funahashi, MD, PHD,§ Hitonobu Tomoike, MD, PHD,* Masafumi Kitakaze, MD, PHD*

Suita, Osaka, Japan

Objectives We investigated the functional relationship between natriuretic peptides and adiponectin by performing both experimental and clinical studies.

Background Natriuretic peptides are promising candidates for the treatment of congestive heart failure (CHF) because of their wide range of beneficial effects on the cardiovascular system. Adiponectin is a cytokine derived from adipose tissue with various cardiovascular-protective effects that has been reported to show a positive association with plasma brain natriuretic peptide (BNP) levels in patients with heart failure.

Methods The expression of adiponectin messenger ribonucleic acid (mRNA) and its secretion were examined after atrial natriuretic peptide (ANP) or BNP was added to primary cultures of human adipocytes in the presence or absence of HS142-1 (a functional type A guanylyl cyclase receptor antagonist). Changes of the plasma adiponectin level were determined in 30 patients with CHF who were randomized to receive intravenous ANP (0.025 μg/kg/min human ANP for 3 days, n = 15) or saline (n = 15).

Results Both ANP and BNP dose-dependently enhanced the expression of adiponectin mRNA and its secretion, whereas such enhancement was inhibited by pre-treatment with HS142-1. The plasma adiponectin level was increased at 4 days after administration of human ANP compared with the baseline value (from 6.56 ± 0.40 μg/ml to 7.34 ± 0.47 μg/ml, $p < 0.05$), whereas there was no change of adiponectin in the saline group (from 6.53 ± 0.57 μg/ml to 6.55 ± 0.56 μg/ml).

Conclusions Natriuretic peptides enhance adiponectin production by human adipocytes in vitro and even in patients with CHF, which might have a beneficial effect on cardiomyocytes in patients receiving recombinant natriuretic peptide therapy for heart failure. (J Am Coll Cardiol 2009;53:2070–7) © 2009 by the American College of Cardiology Foundation

Plasma natriuretic peptide levels are increased in patients with congestive heart failure (CHF), and the measurement of these peptides is used widely to assess the presence, severity, and prognosis of CHF (1,2). Both atrial natriuretic peptide and brain natriuretic peptide (ANP and BNP, respectively) have a beneficial effect in patients with heart failure because of their various biological actions (3–5).

See page 2078

Adiponectin is a circulating cytokine derived from adipose tissue that has attracted considerable interest because of its identification as a risk factor for cardiovascular disease (6,7) and CHF (8). Adiponectin production is down-regulated in patients with coronary risk factors that are associated with the development of heart failure (9,10).

From the Cardiovascular Division of *Medicine and †Biochemistry, National Cardiovascular Center, Suita, Osaka, Japan; and the Departments of ‡Cardiovascular Medicine and §Metabolic Medicine, Osaka University Graduate School of Medicine, Suita, Osaka, Japan. This work is supported by grants-in-aid from the Ministry of Health, Labor, and Welfare-Japan, grants-in-aid from the Ministry of Education, Culture, Sports, Science and Technology-Japan, grants from the Japan Heart Foundation, and grants from the Japan Cardiovascular Research Foundation (all to Dr. Kitakaze) and Takeda Medical Research Foundation (to Dr. Funahashi). Drs. Tsukamoto, Fujita, and Kato contributed equally to this work.

Manuscript received August 27, 2008; revised manuscript received January 22, 2009, accepted February 19, 2009.